

EXPERIMENTAL AND COMPUTATIONAL COMPARISONS OF FAN-SHAPED FILM-COOLING ON A TURBINE VANE SURFACE

W. Colban and K. A. Thole
Mechanical Engineering Department
Virginia Tech
Blacksburg, Virginia, USA

M. Haendler
Siemens Power Generation
Muelheim a. d. Ruhr, Germany

ABSTRACT

The flow exiting the combustor in a gas turbine engine is considerably hotter than the melting temperature of the turbine section components, of which the turbine nozzle guide vanes see the hottest gas temperatures. One method used to cool the vanes is to use rows of film-cooling holes to inject bleed air that is lower in temperature through an array of discrete holes onto the vane surface. The purpose of this study was to evaluate the row-by-row interaction of fan-shaped holes as compared to the performance of a single row of fan-shaped holes in the same locations.

This study presents adiabatic film-cooling effectiveness measurements from a scaled-up, two-passage vane cascade. High resolution film-cooling measurements were made with an infrared (IR) camera at a number of engine representative flow conditions. Computational fluid dynamics (CFD) predictions were also made to evaluate the performance of some of the current turbulence models in predicting a complex flow such as turbine film-cooling. The RNG $k-\epsilon$ turbulence model gave a closer prediction of the overall level of film-effectiveness, while the v^2-f turbulence model gave a more accurate representation of the flow physics seen in the experiments.

INTRODUCTION

The nozzle guide vanes in a gas turbine, located directly downstream of the combustion section, are particularly susceptible to thermal failure, with gas temperatures commonly reaching levels above component latent melting temperatures. Combustion temperatures continue to rise in an effort to increase the efficiency and power output from gas turbine engines. This rise has led to the increased demand to devise better cooling schemes and more resilient materials from which to manufacture the turbine vanes. Many cooling strategies are typically used at the same time; including impingement cooling, internal passage cooling, and external film-cooling.

While designing various cooling configurations, consideration must also be given to the structural integrity of the vanes, since turbine vanes are under extremely high thermal stresses.

Ideally, film-cooling aims to inject cooler temperature fluid over the surface of the vane, shielding it from the high temperature freestream gases. This goal is sometimes difficult to achieve, however, as the nature of the flow through the turbine passage tends to be uncompromising with conditions including high freestream turbulence, secondary flows, high surface curvature, rapid flow acceleration, and high pressure gradients, all of which have been shown to affect cooling performance. Film-cooling offers the engine designer an enticing way to extend part life, however, the use of too much coolant flow from the compressor takes a toll on the overall engine efficiency. To counteract this consequence, engine designers are constantly on the lookout for ways to maintain or even increase the cooling performance but with less coolant.

Alternative hole geometries are sometimes used by engine designers, such as the diffused or so-called fan-shaped holes, to maximize the performance of the injected coolant. By expanding the exit of the cooling hole in the lateral direction, the effective momentum of the surface coolant can be reduced prior to injection. Goldstein et al. [1] showed that fan-shaped holes provide better surface attachment at higher blowing ratios, as well as better lateral spreading of the coolant than cylindrical holes. A slight deviation of this design is the laidback fan-shaped hole, wherein a forward expansion is also included, further inhibiting jet liftoff. The major drawback for non-cylindrical hole geometries is increased initial manufacturing costs. The benefits however, of fan-shaped holes are many, including increased part life (fewer replacements needed), less required coolant (increased engine efficiency), and fewer holes needed (increased structural stability of the vane).

CFD is becoming an essential design tool in the gas turbine

industry, because it is both cheaper and faster than performing experiments. However, in order to rely on CFD results it is first necessary to validate the predictions with measurements to ensure computational reliability. In this study, detailed comparisons of the measured adiabatic effectiveness data are made with CFD predictions using both the RNG k- ϵ and v^2 -f turbulence models.

The standard k- ϵ turbulence model is a Reynolds Averaged Navier-Stokes (RANS) model with two transport equations – one for the turbulent kinetic energy (k) and one for the eddy viscosity (ϵ) – which are used to approximate the turbulent viscosity (μ_t). The RNG k- ϵ model involves renormalization group theory and adds a term to the eddy viscosity transport equation, which makes the model better for high strain flows than the standard k- ϵ model. One major drawback of the RNG k- ϵ model in wall-bounded flows such as film-cooling is the assumption of isotropic turbulence. The existence of the wall introduces anisotropy in the normal fluctuations, the presence of which are not accounted for in the wall functions used to approximate the behavior in the boundary layer in the k- ϵ turbulence models. Wall functions lose their reliability in 3D or separated flow regimes such as sometimes seen in film-cooling.

Durbin [2] incorporated turbulence anisotropy in the near wall region into the existing k- ϵ RANS model by adding two transport equations – one for the normal fluctuations (v^2) and one for an elliptic relaxation function (f) – and effectively removed the necessity of wall functions. The v^2 -f turbulence model correctly models the blocking phenomenon near the wall that is responsible for attenuating the normal turbulent fluctuations, eliminating the requirement of damping functions

in wall bounded flows.

Film-cooling effectiveness has been predicted using both the RNG k- ϵ and the v^2 -f turbulence models in our paper. The complete passage, including the contoured endwall was modeled in the RNG k- ϵ simulation for a baseline case. A spanwise periodic section of the vane passage was modeled using the v^2 -f turbulence model for the same blowing ratios that were measured experimentally.

This study is the first to present detailed high-resolution adiabatic film-cooling effectiveness measurements for a turbine vane with multiple rows of fan-shaped film-cooling holes at engine representative blowing ratios. Contours and laterally averaged values of adiabatic film-cooling effectiveness are presented for both the pressure and suction sides. Adiabatic film-cooling effectiveness data is critical information for engine designers, necessary to predict not only metal temperatures but also to validate CFD predictions.

PAST STUDIES

Because of its crucial role in preventing thermal failure in gas turbine engines, film-cooling has been an extensively researched topic over the last 30 to 35 years ([3],[4]). Flat plate studies have encompassed a variation of every possible geometrical parameter; including surface angle, entrance length, hole spacing, compound angle, lateral expansion angle, forward expansion angle, area ratio, and multiple row configurations. External conditions have also been thoroughly investigated for flat plates; including such effects as turbulence intensity, pressure gradient, and the state of the approaching boundary layer. An excellent review of the relevant shaped hole literature, which primarily focused on flat-plate studies,

NOMENCLATURE

A	area
C	vane true chord
C_D	discharge coefficient
D	film-cooling hole diameter
f	elliptic relaxation function
k	turbulent kinetic energy
k_{cond}	thermal conductivity
m	mass flow rate
M	blowing ratio using local velocity, $M=m_c/A_h U_{local} \rho_{in}$
M_∞	blowing ratio using inlet velocity, $M_\infty=m_c/A_h U_{in} \rho_{in}$
P	hole spacing measured normal to streamwise direction
P	vane pitch
Re	Reynolds number, $Re=U_{in} C/\nu$
s	equivalent slot width, $s=A_{break}/P$
S	distance along the vane surface
t	hole breakout width
T	temperature
U	velocity
v^2	normal velocity fluctuations
X	distance downstream of the hole exit
y^+	wall coordinate
Z	distance measured along the vane span

Greek

α	inclination angle
β	compound angle
ϵ	eddy viscosity, surface emissivity
μ_t	turbulent viscosity
ν	kinematic viscosity
η	adiabatic film-cooling effectiveness, $\eta = (T_\infty - T_{ad}) / (T_\infty - T_c)$
ρ	density
ϕ_1	lateral diffusion angle
ϕ_2	forward expansion angle

Subscripts

ad	adiabatic
break	hole breakout area
c	coolant
exit	hole exit
h	metering area of film-cooling holes based on D
in	inlet condition
local	local conditions
max	maximum
plenum	plenum conditions
surf	surface
∞	freestream conditions

was given by Bunker [5]. Although flat plate studies are a key first step in understanding the flow physics for a given cooling hole geometry, to completely understand the flow physics and evaluate a given film-cooling design, it must be tested on the actual turbine vane. It stands to reason that the flow physics on a highly curved surface such as a turbine vane, coupled with multiple cooling row interaction, could yield results that are different from the flat plate special case. Some studies have presented results for partially and/or fully cooled nozzle guide vanes, but the deficiency of many of those studies is the lack of high resolution effectiveness measurements.

Studies involving a single row of fan-shaped cooling holes on a vane surface have been performed by Zhang et al. [6], Zhang and Pudupatty [7], and Colban et al. [8]. Using the same experimental procedure and facilities for both studies, effectiveness measurements were made with fan-shaped holes on the suction side by Zhang et al. [6] and on the pressure side by Zhang and Pudupatty [7]. Results indicated an increase in effectiveness on the suction side for the blowing ratio range from 0.5 to 1.5 and a decrease in effectiveness on the pressure side for the blowing ratio range from 1.5 to 2.5.

Colban et al. [8] presented adiabatic effectiveness measurements for eight single rows of fan-shaped holes on both the pressure and suction sides in the same facilities as this paper. Their results indicated that in regions of high convex curvature, particularly on the suction side near the leading edge, jet lift-off was prevalent, and increased with blowing ratio. Colban et al. [8] also noted a decrease in effectiveness with increased blowing on the pressure side, which was attributed to partial jet lift-off and hot gas entrainment.

Despite the knowledge gained by studying single row cooling on the vane, it is still necessary to study multiple row film-cooling on the vane. Goldstein et al. [9] showed that on a flat plate a single row of cooling holes separated with increasing blowing ratio, resulting in decreased film-effectiveness. However, with a double row cooling configuration, the upstream row provided the impetus for the downstream row to stay attached to the surface. This resulted in an increased film-effectiveness with blowing ratio. The study by Goldstein et al. [9] suggested that an accurate study of vane film-cooling would not be complete unless all of the engine-present film-cooling rows were tested together.

Effectiveness measurements were made by Guo et al. [10] in a transonic facility for a turbine airfoil with multiple rows of fan-shaped holes. Results showed higher values of effectiveness for fan-shaped holes than for cylindrical holes. However, the decay in effectiveness on the pressure side was faster for fan-shaped than for cylindrical holes, which was most likely the result of a better lateral coverage for the fan-shaped holes. Sargison et al. [11] also measured effectiveness in an annular turbine cascade with multiple rows of cylindrical, fan-shaped, and converging slot holes. They reported similar levels of performance for the fan-shaped and converging slot holes, both of which had superior performance than cylindrical holes.

Effectiveness measurements on the pressure side were

made for three rows of fan-shaped holes and isothermal showerhead blowing by Schnieder et al. [12]. They reported that the presence of isothermal showerhead blowing caused increased mixing of the first pressure side row, lowering effectiveness. However, with showerhead cooling, perhaps the increased mixing of the first pressure side row might actually improve effectiveness. Polanka et al. [13] also studied the effect of showerhead blowing on the first downstream pressure side row, using cylindrical instead of fan-shaped holes. They reported that showerhead blowing caused the jets to stay attached, where they would normally separate without upstream blowing. Polanka et al. [13] suggested that increased turbulent mixing caused by the showerhead dispersed the jet towards the wall, reducing lift-off.

Colban et al. [8] presented effectiveness for fan-shaped holes combined with upstream showerhead blowing. Their results indicated that upstream showerhead blowing increased jet dispersion towards the vane surface for the first row of film-cooling holes downstream on the pressure side, a result consistent with the results of Polanka et al. [13]. Although Colban et al. [8] presented a complete set of high resolution data for single row fan-shaped holes on a turbine vane, it is further necessary to understand the row-to-row interaction, as the state of the approaching boundary layer has been shown to have a significant effect on the performance of a film-cooling jet [14].

There have been a limited number of computational studies involving shaped hole film-cooling on a flat plate. Kohli and Thole [15] used the standard $k-\epsilon$ model with non-equilibrium wall functions to show the importance of modeling the interior plenum conditions correctly. A similar flat-plate study was performed by Hyams and Leylek [16] who investigated the effect of hole geometry on the thermal and flow field using the high Reynolds number $k-\epsilon$ model with generalized wall functions. They showed that laterally diffused shaped holes had the highest adiabatic effectiveness levels downstream of the hole exit location.

Computational film-cooling studies on a turbine vane surface with fan-shaped holes have been done by Hildebrandt et al. [17], Ferguson et al. [18] and Heidmann et al. [19]. Only Heidmann et al. [19] however, modeled more than one row of holes on the vane. Their study used the $k-\omega$ model to simulate a periodic section of the vane with six staggered rows of cylindrical showerhead holes, four rows of fan-shaped holes on the pressure side, and two rows of cylindrical holes on the suction side. The numerical results presented by Heidmann et al. [19] were not validated with experiments, so the validity of the method was not established. The single row numerical results of Ferguson et al. [18] showed good agreement with experimental results for blowing ratios less than 1.5 using the RNG $k-\epsilon$ model with a two-layer wall treatment. Above a blowing ratio of 1.5, the agreement was not so good.

Nothing, to the author's knowledge, as of yet has been published applying the v^2-f turbulence model to film-cooling flow applications. However, because the v^2-f model is valid all

the way to the wall, with no need for wall functions or damping models in the viscous sublayer, it stands to reason that it should be expected to perform at least as good as the existing two-equation models if not better. The v^2 -f model has been used with success in modeling three-dimensional turbulent boundary layers (Parneix et al. [20]) as well as separated flow conditions such as the backward facing step and vortex shedding flows (Durbin [21]).

Of the previous fan-shaped film-cooling studies that have been performed on a vane, the obvious deficiency is for high resolution data for the fully cooled situation. This study offers the first completely cooled turbine vane study with fan-shaped film-cooling giving detailed experimental adiabatic film-cooling effectiveness results. Similarly, past computational studies of film-cooling have been limited in their scope.

EXPERIMENTAL FACILITIES

The experiments were performed in the VTeXCCL large-scale, low-speed, recirculating wind tunnel facility shown in Figure 1. This facility was identical to the one used by Colban et al. [8], and was described in detail by that study. The main features of the facility were a flow split section that divided the flow into two channels; one which was heated to by a 55 kW heater bank and used as the mainstream combustor exit flow and the other which was cooled using a 40 kW chiller in series with a heat exchanger and used as coolant flow.

The test section was a linear, two-passage cascade with a contoured upper endwall. The inlet freestream turbulence intensity was measured to be 1.2% a distance of 0.2 C upstream of the vane leading edge with a hot wire anemometer. Typical mainstream temperature was 60°C, with a nominal difference between the mainstream and coolant of 20°C, yielding a density ratio of 1.06. The pressure at the test section inlet was nearly atmospheric. A list of pertinent geometrical parameters for the test section is given in Table 1, along with certain relevant inlet conditions.

Test Section Design

To match the engine static pressure distribution around the vane to that found in the engine, a contoured surface was implemented for the upper endwall. The contoured endwall, which contracted to roughly 54% of the inlet span height, is shown schematically and graphically in Figure 2. A detailed account of the contour design was given by Colban et al. [8]. The contoured endwall resulted in an excellent match of the experimental static pressure distribution at the midspan to that of the engine. Also, since this investigation was not focused on any three-dimensional effects of the contour on the vane cooling, a rigorous investigation, including CFD predictions and experimental examination, was used to verify the presence of a two-dimensional flow regime in the area where the measurements were taken. All of the film-cooling effectiveness measurements were made between 5% and 32% span, while the flow was essentially two-dimensional below 40% span.

A schematic of the vane test section is shown in Figure 3.

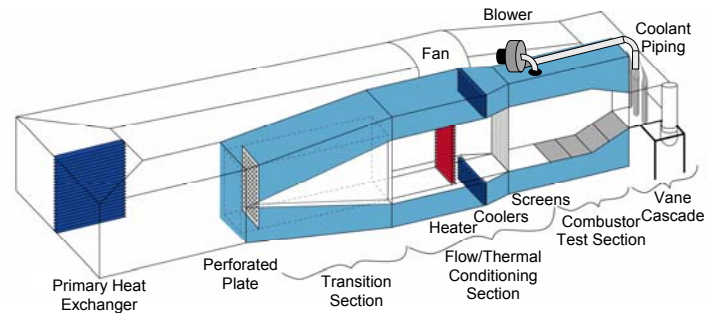


Figure 1. Schematic of the low-speed recirculating wind tunnel facility.

Table 1. Operating Conditions and Vane Parameters

Scale	3X
C (m)	0.53
$S_{max,PS}$ (m)	0.52
$S_{max,SS}$ (m)	0.68
U_{inlet} (m/s)	10
Re_{inlet} (-)	3.0×10^5
ΔT_{FC} (°C)	20
Vane Pitch (m)	0.465

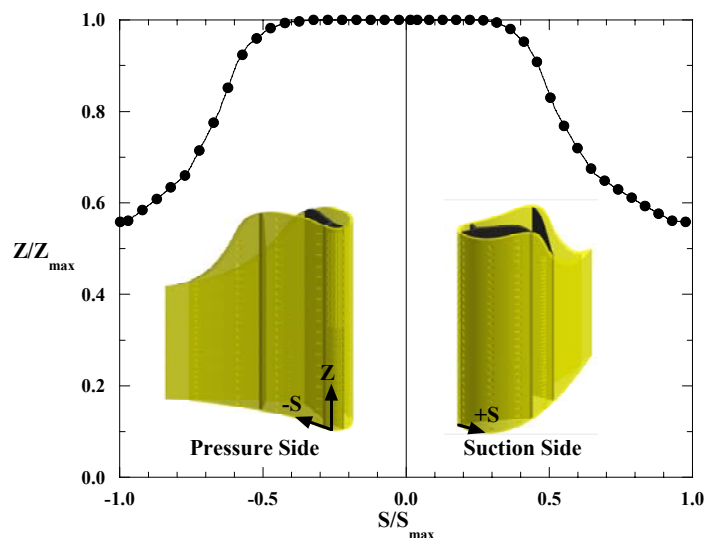


Figure 2. Contoured endwall surface definition.

Bleed valves were used to ensure flow periodicity between the two passages, and the flexible wall was used to make minor adjustments to the flow distribution around the center vane. Also shown in Figure 3 are the plenum locations relative to the holes, as well as the hole designations, to be used throughout the rest of the report.

A detailed discussion of the vane design and construction was given by Colban et al. [8]. The vane contained four interior plenums, which allowed for flow rate control amongst the rows of holes to obtain the desired blowing ratio distribution. Coolant was supplied to the plenums from the upper channel in the wind tunnel using the blower shown in

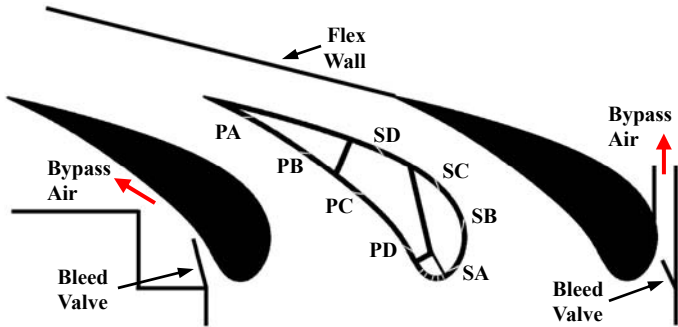


Figure 3. Schematic of experimental test section.

Figure 1. Discharge coefficients, which were presented in the study of Colban et al. [8], were used to set the combined flow rates through each plenum based on the desired blowing ratios.

The test vane contained showerhead cooling with five in-line rows, four fan-shaped pressure side rows, and four fan-shaped suction side rows of film-cooling holes. The diameter of the cylindrical inlet section of the fan-shaped holes was 0.38 ± 0.015 cm. The diameters of each hole were measured to verify that the correct flow area was used to determine the total mass flow rate and individual blowing ratios because of slight manufacturing variation resulting from the five-axis water-jet machining process. Slight variations did occur in fan-shape of the holes as a result of the manufacturing process. Some hole-to-hole variation can be seen in the effectiveness contours, which were attributed to variation in hole shape as well as experimental uncertainty. An illustration of the fan-shaped hole geometry is shown in Figure 4, and relevant parameters for the film-cooling holes are listed in Table 2. The cylindrical showerhead holes had fairly high surface inclination angle of 60° along with a 90° compound angle. The fan-shaped holes had a surface inclination angle of 30° and lateral and forward expansion angles of 10° .

High resolution surface temperature measurements were obtained with an IR camera. Thermocouples placed in the vane surface were used to calibrate the images, which were taken from below the test section at 45° relative to the surface for optical access. Post-processing of the images required a three-dimensional transformation, calibration, conduction correction, and assembly. A detailed description of the complete measurement technique can be found in Colban et al. [8].

Two blowing ratios were defined for this study. For the showerhead region, blowing ratios are reported based on inlet velocity, U_{in} ,

$$M_\infty = \frac{\dot{m}_c}{A_n U_{in} \rho_{in}} \quad (1)$$

For the fan-shaped holes however, it is more appropriate to report blowing ratios in terms of local velocity, U_{local} ,

$$M = \frac{\dot{m}_c}{A_h U_{local} \rho_{in}} \quad (2)$$

Three sets of blowing ratios were measured for the fan-shaped holes, while the showerhead blowing ratio of $M_\infty = 2.0$ was held constant for all cases. The range of measured blowing

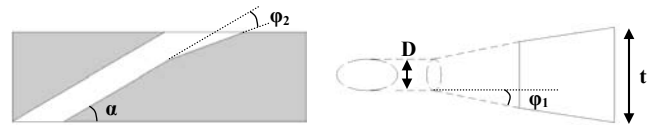


Figure 4. Fan shaped cooling hole detailed geometry.

Table 2. Film-Cooling Hole Parameters

Fan Shaped		Showerhead	
D (cm)	0.38	D (cm)	0.24
α ($^\circ$)	30	α ($^\circ$)	60
ϕ_1 ($^\circ$)	10	β ($^\circ$)	90
ϕ_2 ($^\circ$)	10	t (cm)	0.48
t (cm)	0.81	t/P (-)	0.22
	t/P (-)	S_{exit}/S_{max} (-)	
Row PA	0.540	-0.840	
Row PB	0.405	-0.615	
Row PC	0.405	-0.384	
Row PD	0.270	-0.135	
Row SA	0.405	0.090	
Row SB	0.405	0.214	
Row SC	0.405	0.345	
Row SD	0.810	0.519	

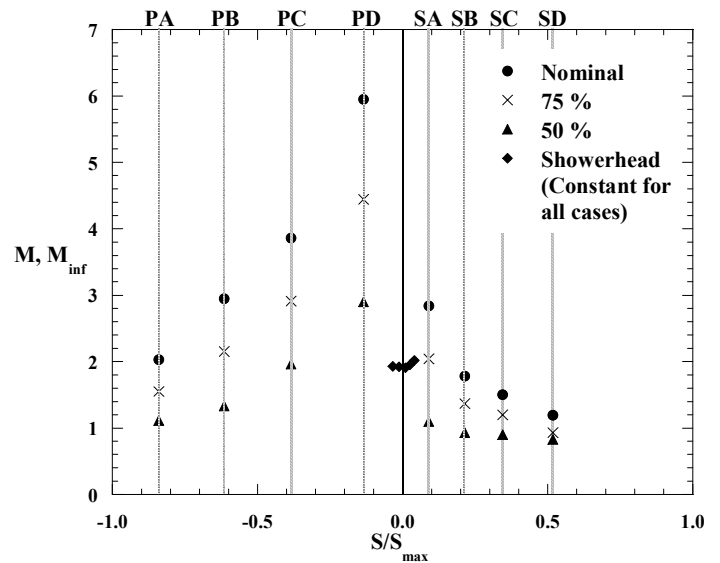


Figure 5. Test matrix of blowing ratios for each case.

ratios, shown in Figure 5, was chosen to encompass typical operating conditions in an industrial gas turbine. As described earlier, blowing ratios were set by using previously measured discharge coefficients.

Experimental Uncertainty

Surface temperatures were measured for a reference case with hot mainstream flow and cool plenum flow, but no surface film-cooling. This procedure yielded values of surface effectiveness without blowing between 0.04 and 0.12. A one-dimensional conduction correction was then applied to the data

using the reference values as described in Etheridge et al. [22]. The partial derivative and sequential perturbation method as explained by Moffat [28] was used to determine uncertainties for the experimentally reported effectiveness values. High values of $\eta = 0.9$ had uncertainties of ± 0.012 , while low values of $\eta = 0.2$ had an uncertainty of ± 0.011 .

COMPUTATIONAL METHODOLOGY

CFD predictions were done with both the RNG $k-\epsilon$ and v^2-f [2] turbulence models. The RNG $k-\epsilon$ was chosen because it is perhaps the most common turbulence model currently used in industry, and serves as a baseline computational comparison for the v^2-f model. The v^2-f model was chosen to see if the improvements made in the near-wall modeling would offer a significant improvement in predictive capability over the current industry standard. The constraints of the two models dictated different approaches in selecting the computational domain and in meshing. All of the CFD predictions were done using Fluent 6.0.1, a commercially available CFD solver with a special module for the v^2-f model.

RNG $k-\epsilon$ Model

The computational domain for the RNG $k-\epsilon$ simulation consisted of one periodic vane passage. A two-dimensional view of the domain is shown in Figure 6. The domain began one chord length upstream of the vane leading edge, using a velocity inlet condition. The exit boundary was located 1.5 C downstream of the trailing edge, a distance suggested by Hermanson and Thole [23] so as not to affect the upstream flow field. The interior plenum geometry was consistent with the experimental setup, using mass flow inlet boundaries. The mass flow rates were specified such that the average blowing ratios exiting the holes would correspond to the experimentally desired values. The contoured endwall was also modeled to see how far down the vane span the effects of the contour reached. The RNG $k-\epsilon$ domain included the entire vane height and all of the cooling holes, 215 of which were fan-shaped holes and 130 of which were cylindrical showerhead holes.

Approximately 2.2 million unstructured tetrahedral cells were used to mesh the domain. This resulted in approximately 1500 volumetric cells to define each fan-shaped hole (Figure 7a), and approximately 400 volumetric cells to define each cylindrical hole. Because the RNG $k-\epsilon$ turbulence model is not valid within the laminar sublayer, non-equilibrium wall functions were used to model the viscous effects of the boundary layer near the wall. This required cells with centroids located within a range of $30 < y^+ < 60$ near the vane surface. Convergence required approximately 1000 iterations on 4 parallel processors. The simulations took approximately two days to converge. Convergence was determined not only from residuals, but also by monitoring area-averaged surface temperatures on both the suction and pressure sides. The drag coefficient around the vane was also monitored as a check on aerodynamic convergence. A grid independence study was also

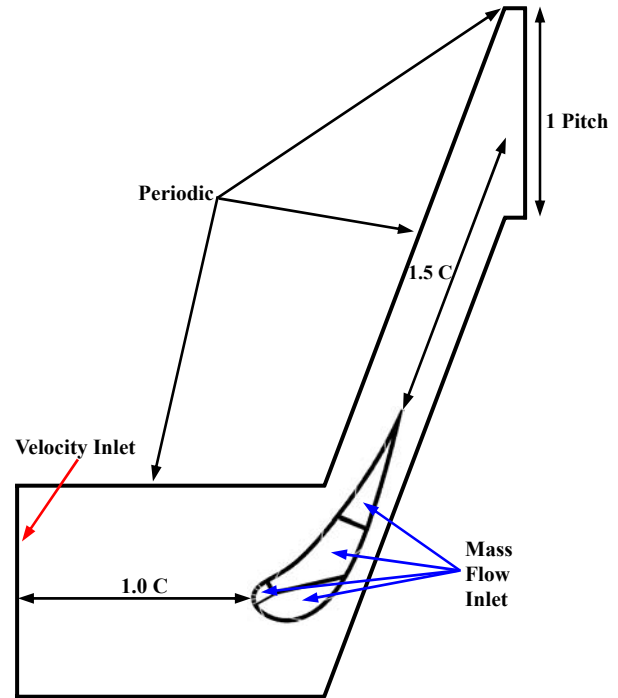


Figure 6. 2D view of the CFD domain (the RNG $k-\epsilon$ model featured the entire span and contour, while the v^2-f prediction featured only a 6 cm spanwise periodic section).

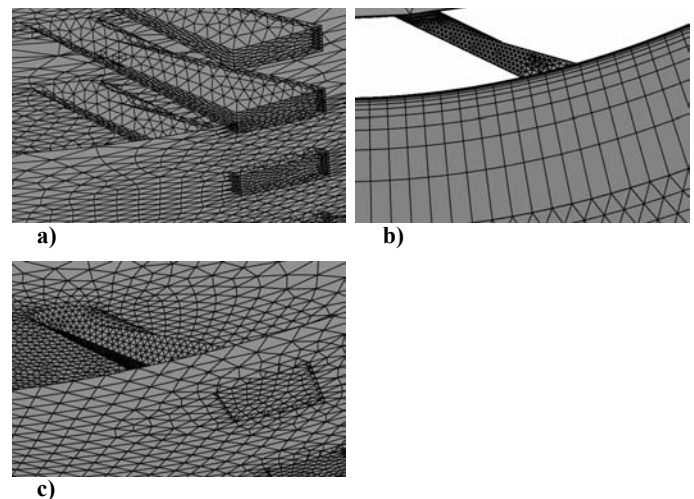


Figure 7. Computational grid sample of (a) the RNG $k-\epsilon$ surface mesh, (b) the v^2-f boundary layer mesh, and (c) the v^2-f surface mesh.

performed by adapting the grid up to 3.9 million cells, but no significant change in results was observed so the initial grid size of 2.2 millions cells was deemed sufficient.

v^2-f Model

Unlike the RNG $k-\epsilon$ model, the v^2-f model is valid to the wall. This required a structured grid in the vicinity of the wall, resolving the boundary layer to within $y^+ < 3$. Consequently, modeling the entire span was not a possibility for the v^2-f

model due to the higher cell density required near the wall. For this reason, only a 6 cm spanwise periodic section was included in the computational domain, which is shown schematically in Figure 6. Both the experimental results and the RNG $k-\epsilon$ CFD results showed periodicity below the midspan, so it was valid to model only the small periodic section, thus making the computations feasible.

The v^2-f model grid contained approximately 1.6 million cells in order to get the near wall resolution. The vane surface was meshed with an unstructured grid, and a boundary layer mesh was applied to the vane surface (shown in Figure 7b). Consequently, there were prismatic cells to a distance of 1.5 cm from the wall, at which point the remainder of the domain was meshed with unstructured tetrahedral cells. The surface mesh resolution is shown for the v^2-f simulations in Figure 7c. Solutions were run for 500 iterations on a first order upwind scheme, before being switched over to a second order upwind scheme with SIMPLEC coupling for 1500 iterations. The v^2-f model computations were run on 3 parallel processors and required approximately 3 days to reach convergence. As with the RNG $k-\epsilon$ model, the surface temperatures and drag coefficient were monitored as additional convergence criteria.

RESULTS

Prior to performing the multiple row adiabatic film-cooling measurements, the experimental method and data reduction procedure were validated for a single row and compared to existing published data. Figure 8 shows laterally averaged single row effectiveness downstream of row SC, a row which was located in a relatively flat region of the vane. Because of differences in hole geometry and spacing, the distance downstream of the hole exit was normalized with respect to the equivalent exit slot width s , where s was the ratio of the hole breakout area to the hole spacing P . The results show excellent agreement with the flat plate study by Gritsch et al. [24], thus validating both the experimental and data reduction methods.

Pressure Side

Adiabatic film-cooling effectiveness contours for each case are shown in Figure 9 for the pressure side. In total, five images were required to completely capture the pressure side, with measurements taken in the nominally 2-D flow region of the vane. The showerhead cooling was largely ineffective at cooling the leading edge region, which Colban et al. [8] attributed to jet lift-off from the high surface angle. The first row of fan-shaped holes showed lift-off by a narrowing in the jet contour just downstream of the hole exit. However, downstream near $S/S_{max} = -0.20$, the jets began to spread laterally. This was a result of the holes in row PD being placed in a region of concave curvature on the pressure side. The jets lifted off initially, but downstream they impinged on the vane surface, which caused lateral spreading. These results were consistent with the cylindrical film-cooling study performed by Ito et al. [25] on a concave pressure surface.

Overall, there was an increase in η with distance from the

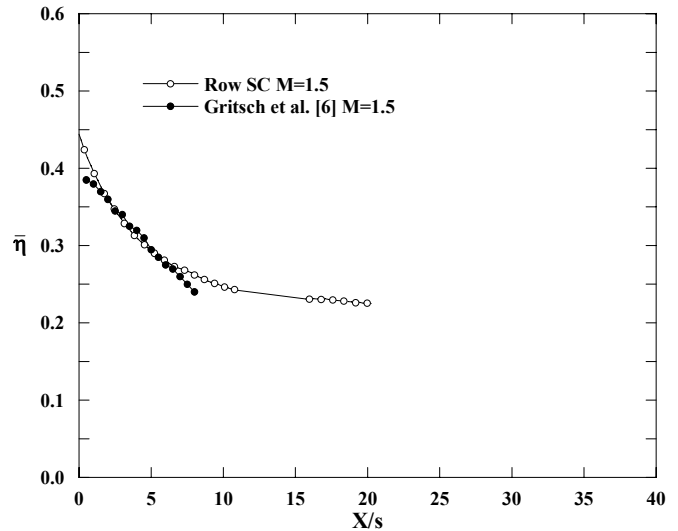


Figure 8. Comparison of results with previously published data.

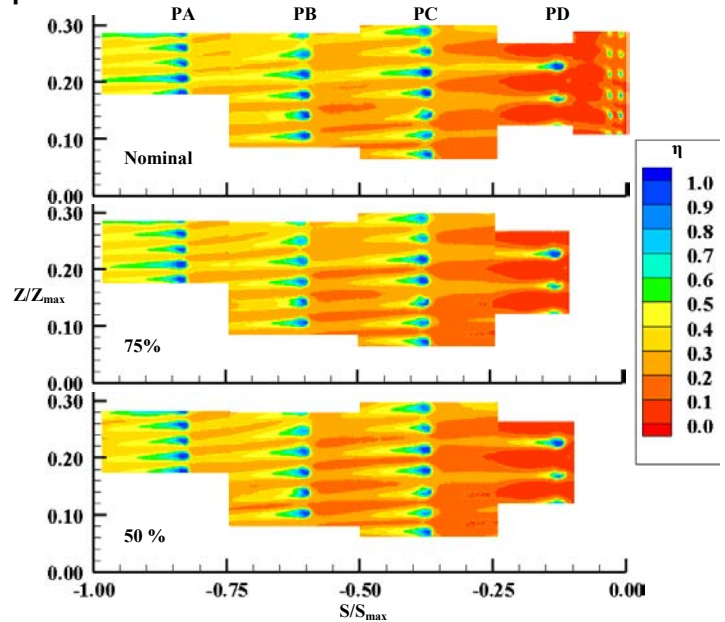


Figure 9. Pressure side experimental results.

leading edge, which is evident from the increased η levels between the jets in rows PC, PB, and PA. Laterally averaged η values (shown in Figure 10) also show an increase in cooling effectiveness with increased blowing. This result differs from the single row results for the pressure side (Colban et al. [8]), which showed a decrease in film-effectiveness with increased blowing. The belief is that the upstream coolant caused increased turbulent mixing in the downstream jet (both laterally and normal to the surface). The enhanced mixing coupled with the upstream coolant caused better film-cooling jet diffusion and consequently more effective surface cooling. Figure 11 shows the single row data from Colban et al. [8] plotted with the multi-row data for the nominal case. The multi-row data has overall much higher η , which became increasingly pronounced with surface distance. The increase in η from

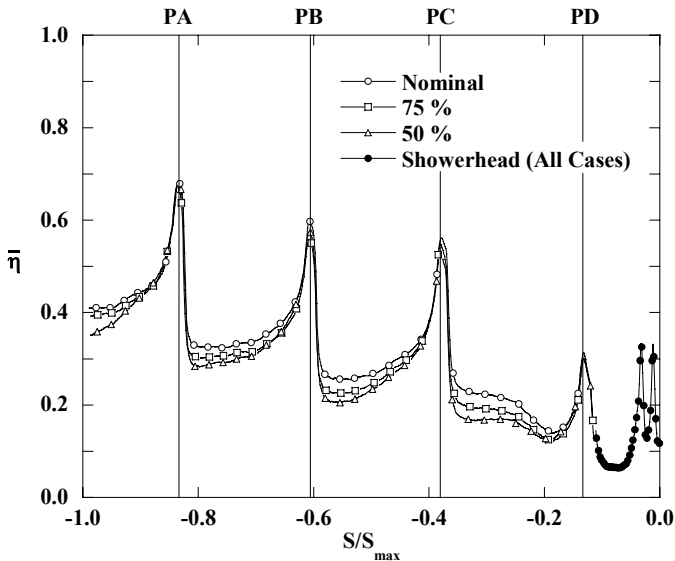


Figure 10. Experimental laterally averaged adiabatic film-cooling effectiveness on the pressure side.

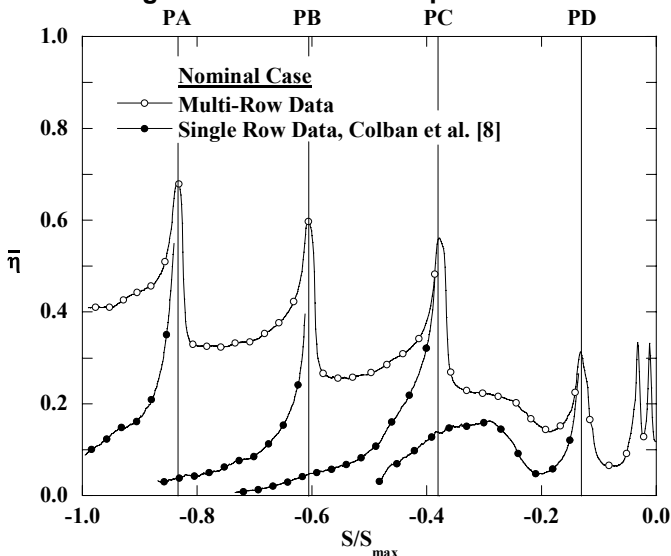


Figure 11. Comparison of multi-row and single row data on the pressure side at nominal conditions.

single row cooling to multi-row cooling is due to a combination of two effects. First, the upstream coolant filled in the gaps or spaces between the downstream rows, leading to a greater cooled surface area. Secondly, as mentioned before, the upstream film-cooling makes the downstream row more effective by increasing the amount of turbulent mixing and reducing the normal momentum. This was particularly evident for row PD, which separated from the surface for both the single row and multi-row tests. The difference however, was that the amount of lift-off was significantly reduced for the multi-row cases, indicating that the upstream showerhead blowing had the effect of keeping the jets attached to the surface. This finding was consistent with the flat-plate study of Goldstein et al. [9] and the airfoil study of Polanka et al. [13], both of which used cylindrical holes.

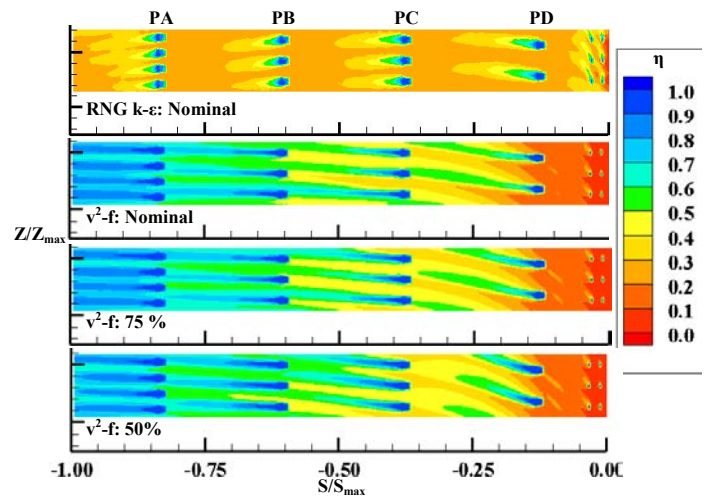


Figure 12. CFD contours for the pressure side.

Computational film-cooling effectiveness contours are shown in Figure 12 for the pressure side. Results from both turbulence models show a spanwise skewness in jet trajectory for row PD (row PC as well for the v^2 -f model). This directionality was caused by the orientation of the showerhead cooling. However, the experimental results did not indicate a directional influence from the showerhead on the downstream rows (Figure 9).

Differences between the two models show that the RNG k - ϵ predictions were more accurate in terms of the overall level of film-cooling effectiveness. However, the RNG k - ϵ prediction showed a wider coolant footprint than the experimental results, while the v^2 -f predictions showed a much narrower coolant footprint similar to the experimental results. Another physical trend shown by the v^2 -f that was not picked up by the RNG k - ϵ prediction was the spreading of the coolant downstream of the first fan-shaped row due to lift-off and reattachment. Neither model accurately predicted the showerhead behavior. The RNG k - ϵ model under-predicted the showerhead lift-off, while the v^2 -f model over-predicted the amount of lift-off in the showerhead region.

A comparison of laterally averaged effectiveness at nominal conditions between the experimental results and both computational models is shown in Figure 13. Again, the RNG k - ϵ model more accurately predicted the overall levels of η , while the v^2 -f model grossly over-predicted η on the pressure side. It is interesting to note that the v^2 -f model predicted a continual rise in effectiveness, indicating a build-up of coolant from upstream rows. The RNG k - ϵ model however, showed no row-to-row increase in effectiveness, which can be seen not only in the laterally averaged values of Figure 13, but in the contour of Figure 12.

The difference in behavior between the two models in the near leading edge region can be seen by examining the streamlines. Streamlines for the nominal blowing conditions are shown in Figure 14 for both turbulence models. The RNG k - ϵ model showed the streamlines stay attached to the surface

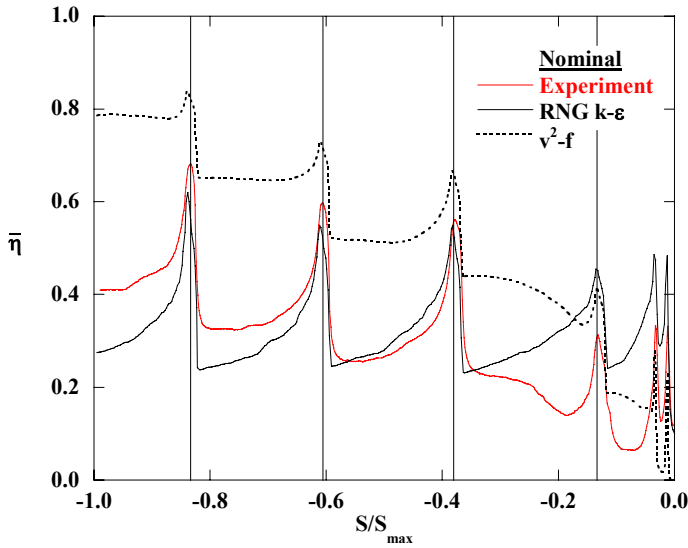


Figure 13. Pressure side comparison of laterally averaged film-effectiveness with computations.

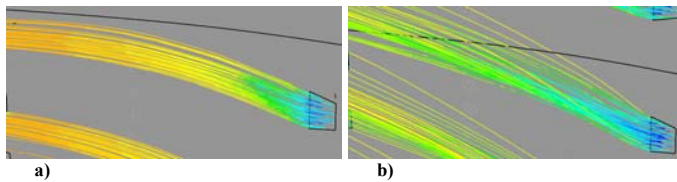


Figure 14. Streamlines near the leading edge for (a) RNG $k-\epsilon$ and (b) v^2-f models at nominal conditions.

with little lateral spreading, while the v^2-f model showed greater lateral spreading after an initial jet lift-off. Also, the skewness in the jets for both models was illustrated by the streamlines as a compound effect from the showerhead film-cooling, which had a 90° compound angle with respect to the main flow.

Suction Side

Contours of η are shown for the experimental results on the suction side in Figure 15. Significant showerhead lift-off occurred, as on the pressure side, causing poor leading edge region cooling. The jets on the first two suction side rows (SA and SB) separated from the surface at high blowing ratios due to the high curvature and acceleration in that region. Overall, η increased with surface distance from the stagnation line on the suction side, as seen from the laterally averaged η values in Figure 16. Near the leading edge, η decreased with blowing ratio because of the jet separation. However, as we progress along the suction side, the curvature decreases, and the amount of lift-off consequently also decreases. This led to a reversal in trend of η with blowing rates by the end of the suction side.

The effect of multiple cooling rows as opposed to the single row results of Colban et al. [8] for the nominal flow conditions are shown in Figure 17. In contrast to the pressure side, where showerhead lift-off also occurred, the effect of the showerhead on the first suction side row was not as significant. On the suction side, the separated showerhead coolant could not remain close enough to the surface to have an effect on the

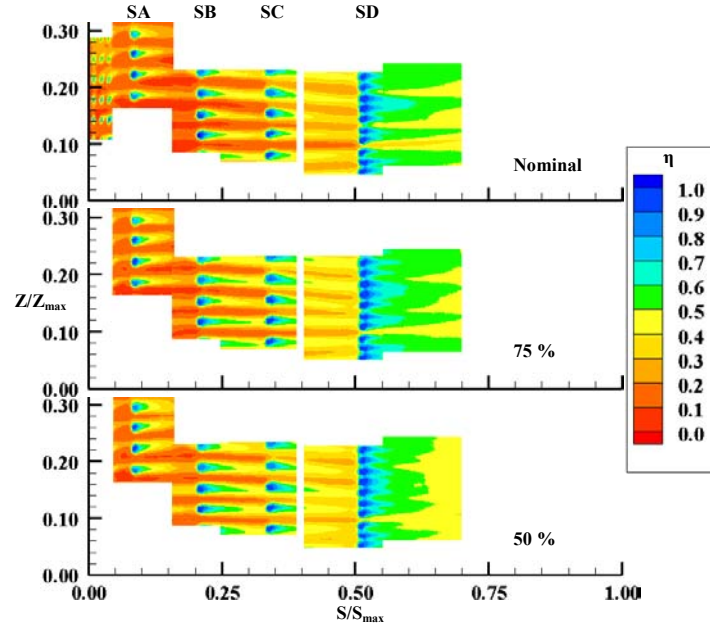


Figure 15. Experimental results on the suction side.

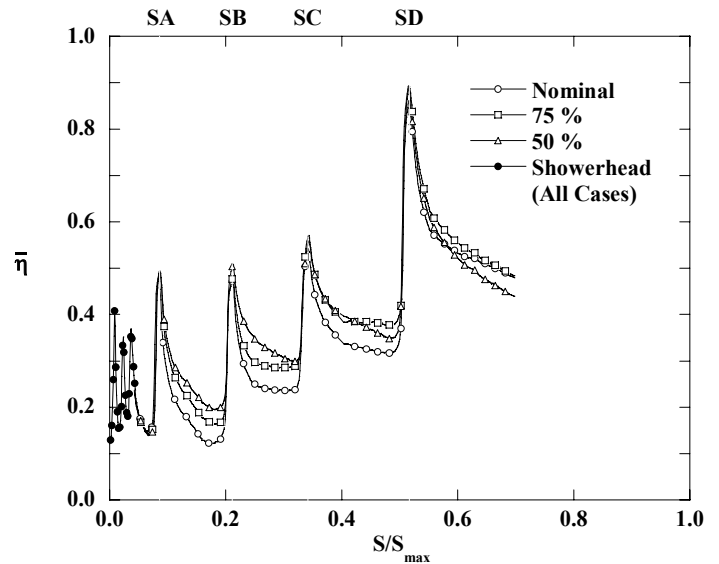


Figure 16. Experimental laterally averaged adiabatic film-cooling effectiveness on the suction side.

downstream rows because of the severe surface curvature. Row SB and SC show a more significant effect of upstream cooling, with results mirroring the trends observed on the pressure side. Further downstream, row SD showed little effect of upstream cooling. This was because of the extremely close hole spacing for row SD, there was no room for extra coolant between the holes.

Contours of η are shown in Figure 18 for the CFD results on the suction side. Just as row PD on the pressure side, row SA was directionally influenced by the showerhead cooling. The v^2-f results mimic the experimental results near the leading edge in that they also predicted lift-off for the first two rows of fan-shaped holes, and that lift-off also increases with blowing

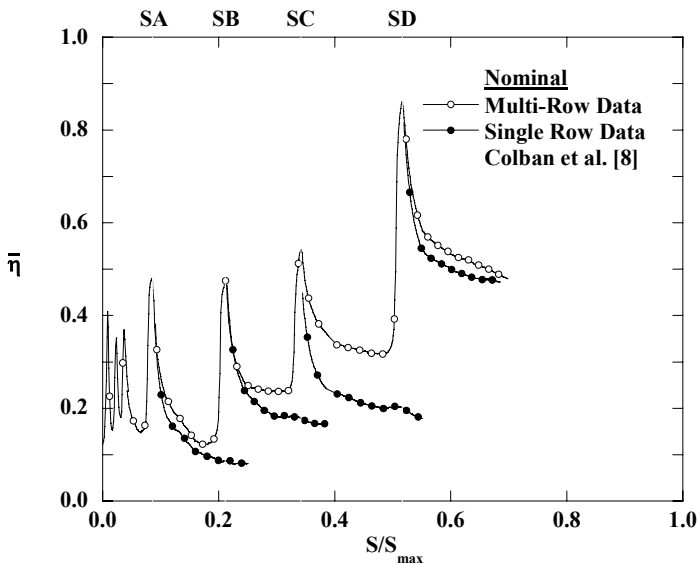


Figure 17. Comparison of multi-row and single row data on the suction side at nominal conditions.

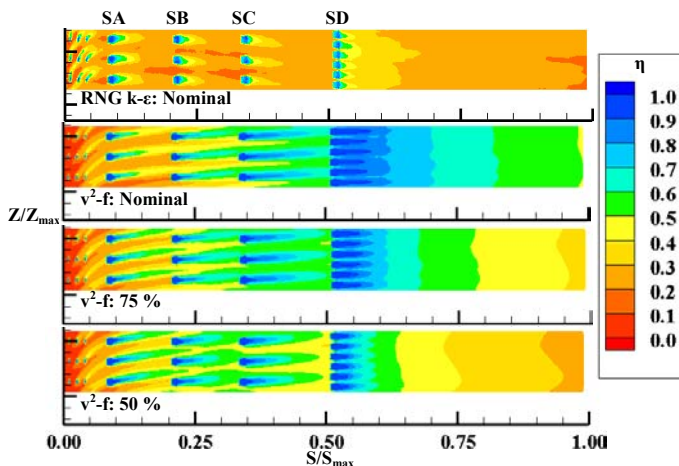


Figure 18. CFD contours for the suction side.

ratio. The v^2 - f model also closely predicts the amount of lift-off in the showerhead region. As shown in the laterally averaged η values for the nominal case in Figure 19, the RNG k - ϵ model exhibits a much faster decay in η downstream of the attached fan-shaped rows than was measured in the experiments. On the other hand, the v^2 - f model exhibits more lateral spreading of the attached jets than was measured experimentally, leading to less decay in η with distance downstream. The streamlines on the suction side (Figure 20) also show the greater lateral spreading of the fan-shaped holes predicted by the v^2 - f model as compared to the RNG k - ϵ model.

CONCLUSIONS

This study presented a detailed experimental and computational investigation of film-cooling on a gas turbine vane with fan-shaped holes. Multi-row data was presented at a range of engine representative blowing ratios on both the pressure and suction sides, and compared to CFD predictions

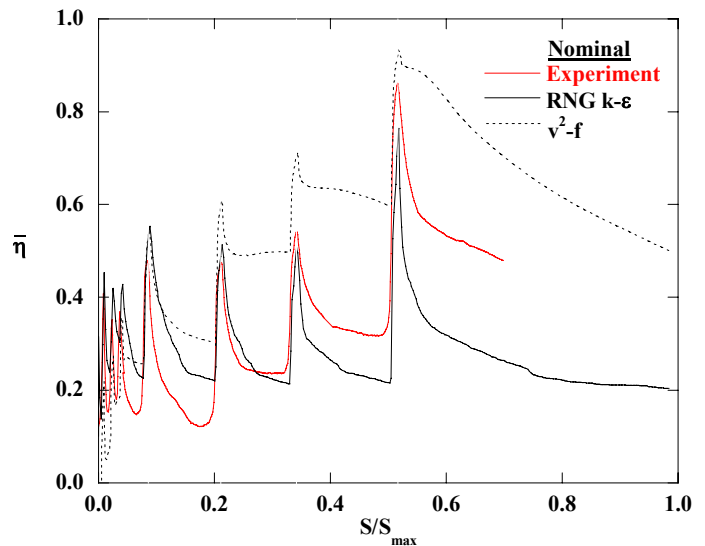


Figure 19. Suction side comparison of laterally averaged film-effectiveness with computations.

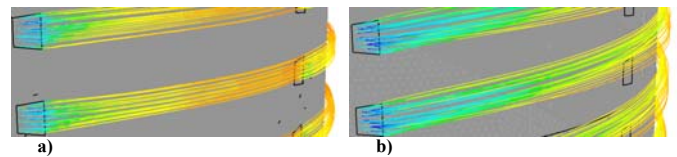


Figure 20. Streamlines near the leading edge for (a) RNG k - ϵ and (b) v^2 - f models at nominal conditions.

using both the RNG k - ϵ and v^2 - f turbulence models.

Experiments showed that on the pressure side the showerhead blowing was not very effective, with excessive lift-off leading to little cooling in that region. Downstream, the first pressure side fan-shaped row exhibited lift-off and reattachment, as evidenced by a narrowing and widening in jet contours, although the lift-off was not as significant as the single row case. Overall, η levels increased on the pressure side with both surface distance and blowing ratio.

Showerhead blowing was also relatively ineffective on the suction side, again exhibiting substantial lift-off and low film-cooling effectiveness. In the near leading edge region of high curvature on the suction side, jet lift-off was accentuated by blowing ratio yielding much lower levels of η at high blowing ratios.

The CFD predictions did not agree well with the experimental results for the most part, at best capturing either the correct η levels or the correct physics, but not both. The v^2 - f model more nearly predicted the actual flow physics, while the RNG k - ϵ model offered a better match with the experimental data in terms of correct effectiveness levels. Although there have been matching CFD predictions for flat plate film-cooling, clearly more advances in CFD turbulence modeling are required before the highly complex flow of film-cooling on a gas turbine vane can be modeled accurately.

ACKNOWLEDGMENTS

The authors are grateful to Siemens Power Generation for

their funding and support of this project.

REFERENCES

- [1] R. J. Goldstein, E. R. G. Eckert, and F. Burggraf, "Effects of Hole Geometry and Density on Three-Dimensional Film Cooling," *ASME Journal of Heat and Mass Transfer*, vol. 17, pp. 595-607, 1974.
- [2] P. A. Durbin, "Near-Wall Turbulence Closure Modeling Without 'Damping Functions'," *Theoretical and Computational Fluid Dynamics*, vol. 3, pp. 1-13, 1991.
- [3] D. M. Kercher, *Film-Cooling Bibliography: 1940-2002*: Private publication, 2003.
- [4] D. M. Kercher, *Film-Cooling Bibliography Addendum: 1999-2004*: Private publication, 2005.
- [5] R. S. Bunker, "A Review of Shaped Hole Turbine Film-Cooling Technology," *ASME Journal of Heat Transfer*, vol. 127, pp. 441-453, 2005.
- [6] L. Zhang, M. Baltz, R. Pudupatty, and M. Fox, "Turbine Nozzle Film-Cooling Study Using the Pressure Sensitive Paint (PSP) Technique," 99-GT-196, 1999.
- [7] L. Zhang and R. Pudupatty, "The Effects of Injection Angle and Hole Exit Shape on Turbine Nozzle Pressure Side Film-cooling," 2000-GT-247, 2000.
- [8] W. Colban, A. Gratton, K. A. Thole, and M. Haendler, "Heat Transfer and Film-Cooling Measurements on a Stator Vane with Fan-Shaped Cooling Holes," GT2005-68258, 2005.
- [9] R. J. Goldstein, E. R. G. Eckert, H. D. Chiang, and E. Elovic, "Effect of Surface Roughness on Film Cooling Performance," *ASME Journal of Engineering for Gas Turbines and Power*, vol. 107, pp. 111-116, 1985.
- [10] S. M. Guo, C. C. Lai, T. V. Jones, M. L. G. Oldfield, G. D. Lock, and A. J. Rawlinson, "The Application of Thin-Film Technology to Measure Turbine-Vane Heat Transfer and Effectiveness in a Film-Cooled, Engine-Simulated Environment," *International Journal of Heat and Fluid Flow*, vol. 19, pp. 594-600, 1998.
- [11] J. E. Sargison, S. M. Guo, M. L. G. Oldfield, G. D. Lock, and A. J. Rawlinson, "A Converging Slot-Hole Film-Cooling Geometry Part 2: Transonic Nozzle Guide Vane Heat Transfer and Loss," 2001-GT-0127, 2001.
- [12] M. Schnieder, S. Parneix, and J. von Wolfersdorf, "Effect of Showerhead Injection on Superposition of Multi-Row Pressure Side Film-Cooling with Fan Shaped Holes," GT2003-38693, 2003.
- [13] M. D. Polanka, M. I. Ethridge, J. M. Cutbirth, and D. G. Bogard, "Effects of Showerhead Injection on Film Cooling Effectiveness for a Downstream Row of Holes," 2000-GT-240, 2000.
- [14] H. Riess and A. Böles, "The Influence of the Boundary Layer State and Reynolds Number on Film-cooling and Heat Transfer on a Cooled Nozzle Guide Vane," 2000-GT-205, 2000.
- [15] A. Kohli and K. A. Thole, "A CFD Investigation on the Effects of Entrance Crossflow Directions to Film-Cooling Holes," *32nd National Heat Transfer Conference*, vol. 12, pp. 223-232, 1997.
- [16] D. G. Hyams and J. H. Leylek, "A Detailed Analysis of Film Cooling Physics Part III: Streamwise Injection with Shaped Holes," 97-GT-271, 1997.
- [17] T. Hildebrandt, W. Ganzert, and L. Fottner, "Systematic Experimental and Numerical Investigations on the Aerothermodynamics of a Film Cooled Turbine Cascade with Variation of the Cooling Hole Shape Part II: Numerical Approach," 2000-GT-298, 2000.
- [18] J. D. Ferguson, J. H. Leylek, and F. A. Buck, "Film Cooling on a Modern HP Turbine Blade Part III: Axial Shaped Holes," GT-2002-30522, 2002.
- [19] J. D. Heidmann, A. J. Kassab, E. A. Divo, F. Rodriguez, and E. Steinthorsson, "Conjugate Heat Transfer Effects on a Realistic Film-Cooled Turbine Vane," GT2003-38553, 2003.
- [20] S. Parneix, P. A. Durbin, and M. Behnia, "Computation of 3-D Turbulent Boundary Layers Using the V2F Model," *Flow, Turbulence, and Combustion*, vol. 60, pp. 19-46, 1998.
- [21] P. A. Durbin, "Separated Flow Computations with the $k-\epsilon-v^2$ Model," *AIAA Journal*, vol. 33, pp. 659-664, 1995.
- [22] M. I. Ethridge, J. M. Cutbirth, and D. G. Bogard, "Scaling of Performance for Varying Density Ratio Coolants on an Airfoil with Strong Curvature and Pressure Gradient Effects," 2000-GT-239, 2000.
- [23] K. S. Hermanson and K. A. Thole, "Effect of Inlet Conditions on Endwall Secondary Flows," *Journal of Propulsion and Power*, vol. 16, pp. 286-296, 2000.
- [24] M. Gritsch, A. Schulz, and S. Wittig, "Adiabatic Wall Effectiveness Measurements of Film-Cooling Holes With Expanded Exits," *ASME Journal of Turbomachinery*, vol. 120, pp. 549-556, 1998.
- [25] S. Ito, R. J. Goldstein, and E. R. G. Eckert, "Film Cooling of a Gas Turbine Blade," *Journal of Engineering for Power*, vol. 100, pp. 476-481, 1978.